PHILOSOPHICAL TRANSACTIONS OF THE ROYAL SOCIETY A

rsta.royalsocietypublishing.org

Research

**Cite this article:** Isakov M, Hiermaier S, Kuokkala V-T. 2014 Improved specimen recovery in tensile split Hopkinson bar. *Phil. Trans. R. Soc. A* **372**: 20130194.
http://dx.doi.org/10.1098/rsta.2013.0194

One contribution of 11 to a Theme Issue 'Shock and blast: celebrating the centenary of Bertram Hopkinson's seminal paper of 1914 (Part 2)'.

**Subject Areas:**
materials science, mechanical engineering

**Keywords:**
tensile split Hopkinson bar, specimen recovery, numerical analysis

**Author for correspondence:**
Veli-Tapani Kuokkala
e-mail: veli-tapani.kuokkala@tut.fi

# Improved specimen recovery in tensile split Hopkinson bar

Matti Isakov[1,2,†], Stefan Hiermaier[1] and Veli-Tapani Kuokkala[2]

[1]Fraunhofer Institute for High-Speed Dynamics, Ernst-Mach-Institut, Eckerstrasse 4, 79104 Freiburg, Germany
[2]Department of Materials Science, Tampere University of Technology, PO Box 589, 33101 Tampere, Finland

This paper presents an improved specimen recovery method for the tensile split Hopkinson bar (TSHB) technique. The method is based on the trapping of residual stress waves with the use of momentum trap bars. As is well known, successful momentum trapping in TSHB is highly sensitive to experimental uncertainties, especially on the incident bar side of the set-up. However, as is demonstrated in this paper, significant improvement in the reliability of specimen recovery is obtained by using two momentum trap bars in contact with the incident bar. This makes the trapping of the reflected wave insensitive to striker speed and removes the need for a precision set gap between the incident bar and the momentum trap.

## 1. Introduction

The ability to interrupt a mechanical loading test is often needed when one wants to study the microstructural evolution of the test material or impart changes to the deformation path. This task is almost trivial at quasi-static strain rates, but becomes increasingly complex when the strain rate is increased owing to the loss of closed-loop control of the loading device and the introduction of dynamic effects, such as inertia of moving parts and stress wave propagation. The split Hopkinson bar (SHB) technique is well established as a means of materials testing near a strain rate of $1000\,s^{-1}$. In terms of interrupting the loading at a predetermined moment, the main challenge in SHB testing is protecting the specimen from residual stress waves, which are inherent to the technique. The task is particularly challenging in

[†]Visiting researcher at affiliation 1. On leave of absence from affiliation 2.

Royal Society Publishing

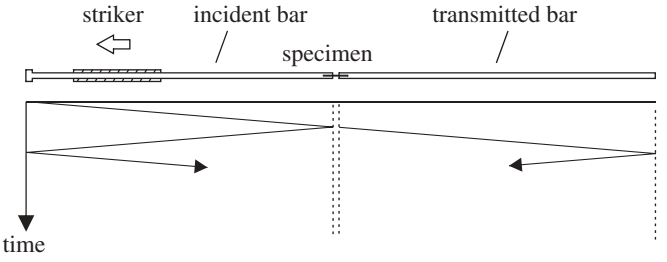


**Figure 1.** Schematic of the wave motion in a TSHB test without momentum trapping.

tensile split Hopkinson bar (TSHB) testing, because the specimen has to be firmly fixed to the test set-up using adhesives, bolts, etc. This makes the specimen susceptible to both tensile and compressive loads.

In general, there are two different means of specimen protection in TSHB: (i) the use of a rigid fixture around the specimen [1–3] so that specimen deformation is limited and further loading is carried by the protective fixture or (ii) removal or 'trapping' of the stress waves in the set-up after the desired loading event [4–6]. The main challenge in the first option is the design of the protective fixture so that it does not interfere with stress wave propagation before the actual specimen recovery [2]. Furthermore, the protective fixture tends to limit the use of external temperature control devices and digital image correlation techniques. The second option is preferable because the loading event before the recovery is similar to a conventional TSHB test, that is, the equations for data analysis are unchanged and the specimen is free from any surrounding objects. The main challenge of successful wave trapping, however, is the high degree of accuracy required in the test set-up. This paper presents a new version of momentum trapping in TSHB, which improves the reliability of specimen recovery compared to the existing techniques [4–6]. The technique is based on the use of two momentum traps instead of only one for the trapping of the reflected wave. This approach was recently proved feasible in compression by Prot *et al*. [7].

## 2. Analytical basis

The method presented in this paper is a modification to a striker-based TSHB set-up shown schematically in figure 1. As shown in the figure, the impact of the striker on the flange at the left end of the incident bar creates a tensile stress wave, called hereafter the 'incident wave', which propagates towards the specimen. When the incident wave reaches the specimen, part of it is reflected back as a wave of compression ('reflected wave'), while the rest propagates to the transmitted bar as a wave of tension ('transmitted wave'). As figure 1 depicts, in a conventional TSHB test the reflected and transmitted waves reflect back from the free ends of the bars and reload the specimen. Therefore, had the specimen not failed during the first loading event, the subsequent reloading can cause further deformation in the specimen. The amplitude of the transmitted wave is proportional to the force carried by the specimen during the first loading. Thus, even partial trapping of the transmitted wave is usually enough to prevent further deformation or buckling of the specimen caused by the residual waves on the transmitted bar side. However, the reflected wave has an amplitude comparable to the incident wave and, thus, the residual waves on the incident bar often cause severe further loading of the specimen unless removed from the bar.

Figure 2 presents the specimen recovery technique used by some of the previous authors [4–6]. This method will, in this paper, be referred to as the 'single trap' method. The residual waves are trapped from the bars using a momentum trap tube on the transmitted bar side and a single trap bar on the incident bar side. The transmitted wave trap is relatively simple to implement,

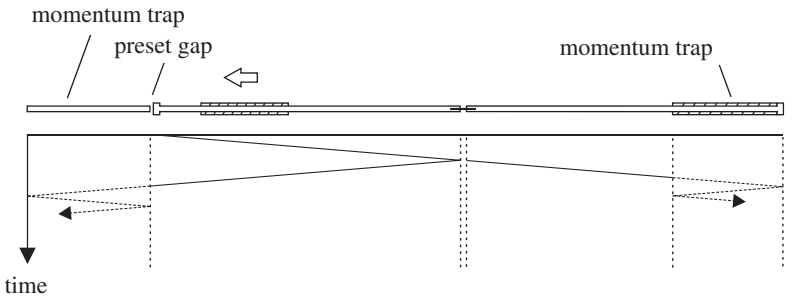


**Figure 2.** Schematic of the wave motion in a TSHB test with conventional momentum trapping.

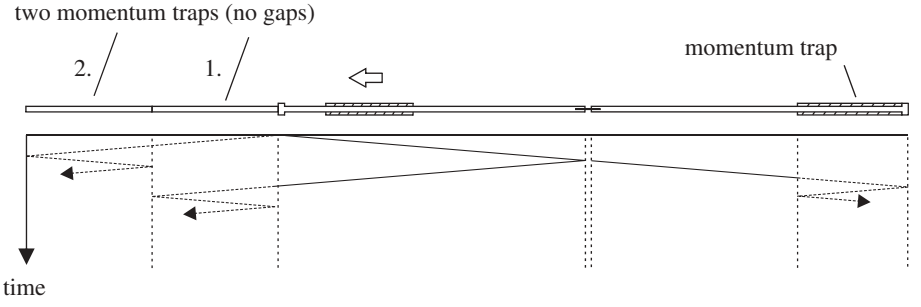


**Figure 3.** Schematic of the wave motion in a TSHB test with the proposed momentum trapping.

since the trap tube can be placed in direct contact with the flange at the end of the transmitted bar. However, on the incident bar side the trap bar has to be set at a precise distance away from the incident bar. As will be shown later, the experimental setting of the gap between the bars is the most critical step of this technique. Assuming that the gap is correctly set, the impact of the striker on the incident bar flange causes bar motion that closes the gap precisely at the end of the incident wave generation. Then, when the reflected wave reaches the end of the incident bar, it is transmitted to the momentum trap instead of being reflected back as a 'new' loading wave.

The success of a recovery test depends on setting the gap width as close as possible to the ideal value, which is determined by the striker speed. As noted by Nemat-Nasser *et al*. [4], in practice the correct gap width has to be determined experimentally by trial and error. An analytical estimate for the gap width can be calculated using the basic wave theory. The details of the calculation are presented in appendix A. Based on this estimate, in a typical test where the striker speed is $10\,\mathrm{m\,s^{-1}}$, loading duration $200\,\mu\mathrm{s}$ and the cross-sectional areas of the striker and the incident bar are identical, the correct gap width is around 1 mm. As will be shown later by a parametric study, the fact that the gap width has to be set with submillimetre accuracy based on *a priori* knowledge of the striker speed makes this technique very sensitive to experimental uncertainties. Van Slycken [5] estimated that the required accuracy in the gap width setting should be at least $50\,\mu\mathrm{m}$ and addressed the problem by building an electromagnet-based actuator system that adjusted the gap width prior to the striker impact. The drawback of the proposed method was, however, the complexity of the system and its reliance on the accurate determination of the striker speed.

In this paper, a completely new solution to the gap width problem is suggested. This method will be referred to below as the 'double trap' method. As figure 3 presents, two momentum trap bars are placed in direct contact with the incident bar. In this set-up, the sequence of events is as follows. The compressive wave created in the flange by the striker impact is transmitted through the first momentum trap bar into the second momentum trap bar (the traps are numbered

according to figure 3). When this compressive wave reflects back as a wave of tension, it is trapped inside the second momentum trap bar since the boundary between the traps carries only compressional loading. This leaves the first momentum trap free of any wave motion and in direct contact with the incident bar, i.e. at this point the situation corresponds to the previously presented recovery technique [4–6] with an ideal gap width. It should be noted that, since no gaps are involved in the test set-up, the proposed technique is insensitive to striker speed. Another difference compared to the conventional method is that part of the incident wave amplitude is 'lost' to the momentum trap bar and thus higher striker speed has to be used to obtain the same specimen strain rate. As can be deduced from figure 3, the critical part of the proposed technique is obtaining perfect contact between the two momentum traps. A gap between the traps will lead to wave reflection within the first trap, which may prematurely separate the trap from the flange. However, ensuring good contact between two bars is experimentally more straightforward than adjusting a preset gap within a fraction of a millimetre, as is required in the single trap method. In contrast to the contact between the two traps, the contact between the first trap and the flange is less critical, since a small gap will close during the striker impact. The drawback is, though, that in that case the incident wave amplitude will show a stepwise decrease, since part of the wave is suddenly transferred to the flange when the gap closes.

## 3. Numerical simulations

Numerical simulations of the above described test set-ups were carried out at the Ernst Mach Institute using Abaqus/Explicit 6.11. Axisymmetric models of both the incident bar side as well as the full test set-up were built using solid elements CAX4R with on average 10 elements across the radius of the TSHB bars and five elements across the radius of the specimen. The bars and momentum traps were modelled as isotropic linear elastic solids, while the specimen material was described with an isotropic elastic–plastic linear strain hardening material model (Young's modulus and Poisson's ratio 200 GPa and 0.3, respectively; yield strength 600 MPa; flow stress at 0.4 plastic strain 1200 MPa). The dimensions and materials of the TSHB set-up and the specimen corresponded to the actual test set-up described in the Experimental part of this paper (§4). It should be noted that in the actual recovery experiments the specimens had a rectangular cross section (area 8 $mm^2$), while in the axisymmetric simulations a round specimen with matching cross-sectional area was used.

The numerical simulations were used to study the effect of experimental variables on the success of the specimen recovery. These variables included changing the striker speed in the single trap technique, as well as introducing gaps between the momentum traps and the flange in the double trap technique. The quality of the recovery was assessed by comparing the residual waves with the original incident wave in terms of bar end motion and specimen deformation. Table 1 summarizes the results of the simulations. As can be seen, the simulations agree well with the qualitative predictions of the analytical analysis. Table 1*a* shows the results of the simulations carried out without the specimen. Based on these simulations, in the single trap technique as little as 5–10% deviation from the successful gap width–striker speed combination results in a failure of the recovery process in terms of the motion of the incident bar. Figure 4 exemplifies the effect of a variation in the striker speed. In figure 4*a*, the speed is nearly optimal and the motion of the flange closes the initial gap without excessively loading the trap bar. By contrast, in figure 4*b* the striker speed is 5% higher and the flange hits the trap already during the striker impact. This sets the trap into motion, which reintroduces the gap. The gap does not close again until the reflected wave reaches the flange and causes motion. This, however, leads to partial reflection of the reflected wave as a new loading wave, thus resulting in a failed recovery. Similarly, if the preset gap is too wide compared with the striker speed, the gap does not close until part of the reflected wave has already reflected back as a new loading wave. Based on the simulations, the former case (too narrow initial gap) is more critical than the latter, since, as exemplified by figure 4*b*, the premature closure of the initial gap will result in a large reintroduced gap by the time the reflected wave reaches the flange. It should be noted, however, that the overall success

**Table 1.** Results of the simulations carried out with (*a*) models of the incident bar side of the test set-up and (*b*) models of the full test set-up. The width of the initial gap in the single trap method as well as the impact speed of the striker in both methods are indicated in the first column.

| set-up | displacement of the flange during striker impact (mm) | after first residual wave reflection | after five residual wave reflections |
|---|---|---|---|
| (*a*) | | relative increase in bar end displacement (%) | |
| no recovery, 10.0 m s$^{-1}$ | 1.01 | 100 | 500 |
| single trap, 1.00 mm gap, 11.0 m s$^{-1}$ | 1.06 | 29.5 | 147 |
| single trap, 1.00 mm gap, 10.5 m s$^{-1}$ | 1.03 | 14.7 | 73.4 |
| single trap, 1.00 mm gap, 10.0 m s$^{-1}$ | 1.00 | 0.8 | 4.0 |
| single trap, 1.00 mm gap, 9.5 m s$^{-1}$ | 0.95 | 2.4 | 12.0 |
| single trap, 1.00 mm gap, 9.0 m s$^{-1}$ | 0.90 | 5.3 | 26.6 |
| double trap, 15.0 m s$^{-1}$ | | −0.5 | −2.3 |
| double trap, 10.0 m s$^{-1}$ | | −0.5 | −2.3 |
| double trap, 5.0 m s$^{-1}$ | | −0.5 | −2.2 |
| double trap, 15.0 m s$^{-1}$ [a] | | −0.4 | −1.6 |
| double trap, 15.0 m s$^{-1}$ [b] | | 9.9 | 49.4 |
| double trap, 15.0 m s$^{-1}$ [c] | | 10.8 | 53.8 |
| (*b*) | | relative increase in specimen strain (%) | |
| no recovery, 10.0 m s$^{-1}$ | 1.01 | 71.3 | — |
| single trap, 1.00 mm gap, 11.0 m s$^{-1}$ | 1.07 | 18.0 | 66.8 |
| single trap, 1.00 mm gap, 10.5 m s$^{-1}$ | 1.04 | 9.2 | 28.3 |
| single trap, 1.00 mm gap, 10.0 m s$^{-1}$ | 1.00 | 0.0 | 0.0 |
| single trap, 1.00 mm gap, 9.5 m s$^{-1}$ | 0.96 | −0.2 | 0.0 |
| single trap, 1.00 mm gap, 9.0 m s$^{-1}$ | 0.90 | 0.1 | 0.1 |
| single trap, 1.00 mm gap, 8.5 m s$^{-1}$ | 0.86 | 0.8 | 2.6 |
| single trap, 1.00 mm gap, 8.0 m s$^{-1}$ | 0.80 | 5.6 | 15.0 |
| double trap, 15.0 m s$^{-1}$ | | 0.0 | 0.0 |
| double trap, 10.0 m s$^{-1}$ | | 0.0 | 0.1 |
| double trap, 15.0 m s$^{-1}$ [a] | | 0.0 | 0.0 |
| double trap, 15.0 m s$^{-1}$ [b] | | 2.3 | 6.4 |

[a]0.05 mm gap between flange and first momentum trap.
[b]0.05 mm gap between first and second momentum traps.
[c]0.1 mm gap between first and second momentum traps.

of the recovery process depends also on the load-carrying capacity of the specimen. As seen in table 1*b*, which lists the results of the simulations carried out with a model of the full test set-up, the specimen is not necessarily plastically deformed by the residual waves even if the gap width does not fully match the striker speed. For example, for initial gap width of 1.00 mm and striker speed of 9.0 m s$^{-1}$, the simulation without the specimen (table 1*a*) indicates a 27% increase in the displacement of the incident bar end after five residual wave reflections. By contrast, for the same gap width and striker speed, the simulation with the specimen and the transmitted bar (table 1*b*) indicates that the residual waves are unable to cause plastic deformation in the specimen.

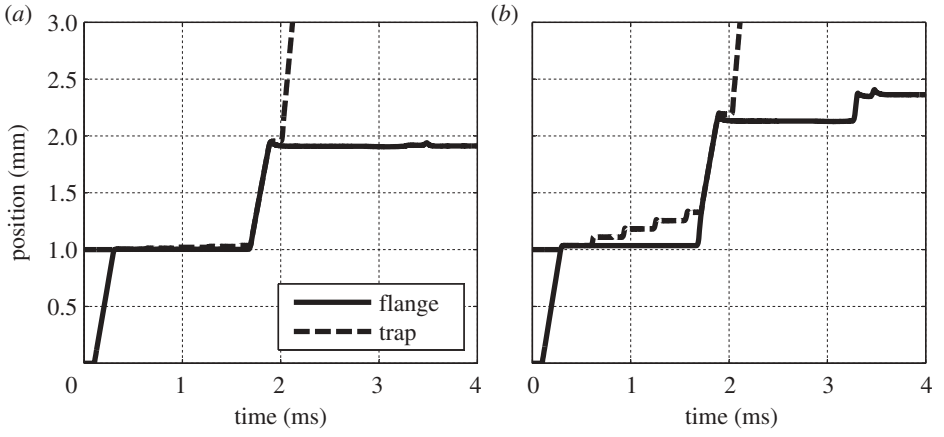


**Figure 4.** Simulation of the single trap recovery technique, motion of the components in the flange–momentum trap interface for 1 mm initial gap width: (*a*) striker speed 10 m s$^{-1}$ and (*b*) striker speed 10.5 m s$^{-1}$.

Table 1 shows how the quality of the recovery in the double trap method is independent of the striker speed. As noted above, this is due to the fact that all components are initially in contact with each other. Thus, compressional waves are fully transmitted across the boundaries regardless of their amplitude. Figure 5 illustrates the results of a simulation for striker speed 15 m s$^{-1}$. The first momentum trap stays in contact with the flange during the striker impact (between 0.1 and 0.3 ms in figure 5*a*), then during the time the incident wave travels to the specimen and reflects back (between 0.3 and 1.65 ms) and finally during the transmission of the reflected wave from the flange to the trap (between 1.65 and 1.85 ms). The first trap does not separate prematurely from the flange because, as shown in figure 5*b*, the initial compressive wave is transmitted to the second momentum trap, which detaches from the first trap after the compressive wave has reflected back as a wave of tension (0.5 ms in figure 5*b*). The simulations showed that this sequence of events was identical for all studied striker speeds. Introduction of a small gap between the flange and the first trap did not markedly change the behaviour of the set-up since the gap closed quickly during the striker impact. By contrast, a gap between the traps led to failed recovery because the compressive wave in the first trap was not completely transferred to the second trap. This resulted in a situation similar to figure 4*b*, i.e. the first trap was detached from the flange before the arrival of the reflected wave.

## 4. Experimental verification

The double trap method presented in this paper was implemented in the TSHB apparatus at the Department of Materials Science, Tampere University of Technology. Referring to figure 3 for schematic visualization, the set-up consists of a 4000 mm by 22 mm diameter incident bar (tempering steel, Young's modulus 210 GPa, Poisson's ratio 0.33, density 7800 kg m$^{-3}$) and a 3000 mm by 22 mm diameter transmitted bar (aluminium alloy, Young's modulus 70 GPa, Poisson's ratio 0.30, density 2700 kg m$^{-3}$). The flange at the end of the incident bar is 20 mm long and has outer diameter of 32 mm. For the recovery experiments, the set-up is fitted with a 500 mm by 22 mm inner diameter by 32 mm outer diameter striker tube (tempering steel), a 800 mm by 27 mm inner diameter by 30 mm outer diameter momentum trap tube (low alloy steel) around the transmitted bar, and two 800 mm by 22 mm diameter (tempering steel) momentum trap bars on the incident bar side. A thin layer of Vaseline is applied to the contacting surfaces of the traps and the bars to ensure that the components stay in contact before the striker impact. In this study, dog-bone sheet specimens (stainless steel EN 1.4318-2B) with 2 mm thickness, 4 mm gauge width and 8 mm gauge length with 2 mm roundings were used. Figure 6 presents an example of the waveform obtained in the recovery experiments. As can be seen in figure 6*a*, the reflected wave

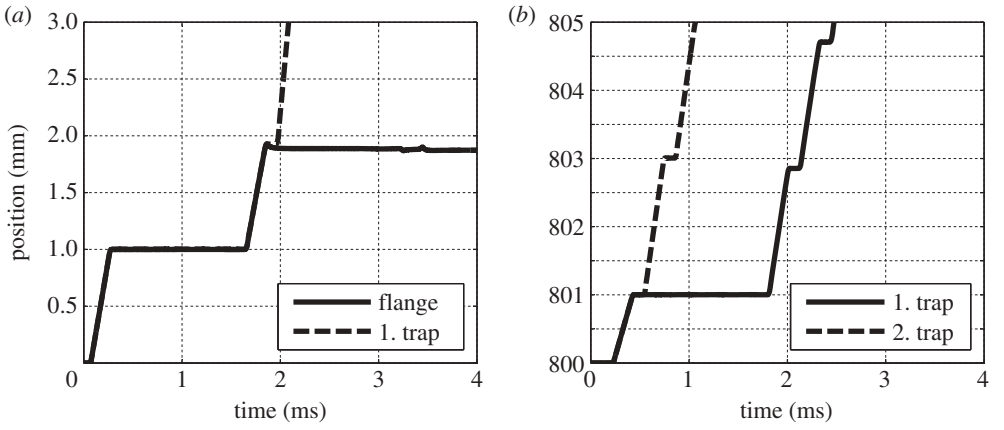


**Figure 5.** Simulation of the double trap recovery technique, striker speed 15 m s$^{-1}$, bar end motion with respect to time: (*a*) components in the flange–first momentum trap interface and (*b*) components in the first momentum trap–second momentum trap interface.

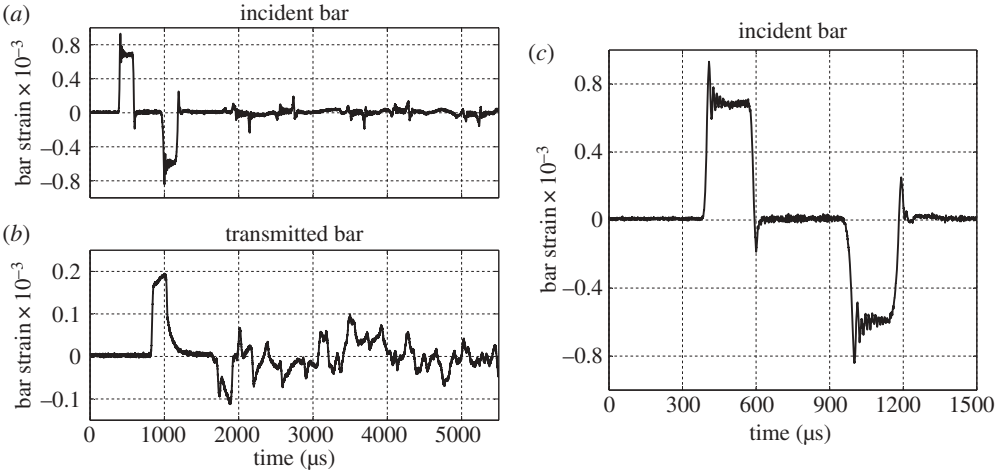


**Figure 6.** Examples of the waveform obtained in the recovery TSHB tests.

is almost completely trapped apart from some minor oscillations. In addition, on the transmitted bar side (figure 6*b*) the residual waves after trapping are below the yield and buckling limits of the specimen. The small compressive wave trailing the incident wave (around 600 μs in figure 6*c*) was later related with the help of simulations to a fillet on the root of the flange–striker boundary. The fillet caused momentarily 'hit and stick' contact between the flange and the striker. As the striker started to move backwards after the impact, for a short moment it dragged the incident bar along, thus causing the compressive wave. However, analysis of the results showed that this compressive wave had negligible influence on the specimen deformation.

The above described test set-up was used for a series of 10 recovery experiments. After each test, the actual deformation of the specimen was manually measured with callipers. In every experiment, the amount of actual specimen deformation equalled or was less than the amount calculated based on stress wave analysis of the first loading event, i.e. conventional HSB analysis of the incident, reflected and transmitted waves. This indicates that during the experiments the specimen was plastically deformed only during the first arrival of the incident wave and that the proposed wave trapping method was sufficient to suppress further specimen deformation. The tendency of the wave analysis to overestimate the specimen elongation of the order of

0.1 mm (with respect to total elongation of around 1.0 mm) was related to the slippage taking place between the specimen and the bars. In contrast to the adhesive joints used normally in the test set-up, in the recovery experiments the specimen was mechanically fixed with bolts into the slits machined into the bar ends. The bolt joint was necessary for the microstructure preserving removal of the specimen, but caused the above-mentioned decrease in the quality of the measured stress waves. A comparison with test results obtained for similar specimens attached by an adhesive showed that, apart from the minor slippage, the measurement of the flow behaviour of the material was not affected by the recovery set-up. It is recommended that recovery experiments are carried out with the use of digital image correlation for strain measurement or that the flow behaviour observed in the recovery experiments is compared with test results obtained with firm specimen attachment, as was done in this study.

## 5. Discussion

Both numerical simulations and experimental tests showed that the complete trapping of the residual waves is difficult. Minor oscillations remain in the bars, for example due to non-ideal contact between the surfaces caused by convex bar ends, alignment errors, etc. Even in ideal circumstances some wave reflection takes place when the reflected wave reaches the flange region, because the flange represents a sudden impedance change on the path of the reflected wave. Part of the wave continues to reflect back at the boundary until equilibrium is reached within the flange by means of wave reverberations. Based on the findings above, it is highly likely that even in the best circumstances the specimen will be reloaded by the residual waves. Since the residual waves continue to travel back and forth in the bars until they decay, even a short-duration wave, if capable of causing plastic deformation, can lead to notable specimen deformation during several wave reverberations in the set-up. Furthermore, after the first loading event it becomes increasingly tedious to calculate specimen stress and strain based on strain gauge signals owing to the motion of several residual waves with different signs and directions.

In this study, a numerical calculation method was used to assess the damage caused by a given residual wave. The method is based on elastic wave calculations within the specimen and is similar to the techniques used by previous authors [8,9] for specimen stress equilibrium calculations. The details of the calculation procedure are given in appendix B. The main idea is that, when the loading wave reaches the specimen, it will take *several wave reverberations within the specimen* before the stress reaches its peak level. Therefore, the specimen can withstand moderate-amplitude waves, i.e. waves that do not cause immediate plasticity in the specimen, if these waves are shorter than the time required for the stress to build up and exceed the yield strength. The calculation method was used to analyse the simulations and experimental tests described above. Limit curves for permissible wave amplitude–wave duration pairs were obtained by repeatedly running the iterative calculations until the maximum allowable force in the specimen was reached. The main advantage of this method is that the damage potential of a given residual wave can be estimated based on a single recording of the wave.

Figure 7 presents a wave amplitude–wave duration limit curve for a specimen similar to that used in the experimental tests. The limit curve corresponds to the force (5 kN) carried by the specimen when it was plastically deformed by the incident wave. Thus, waves whose amplitude and duration lie under the limit curve should cause only elastic loading of the specimen. The upper limit for the amplitude is obtained in the case where the duration of the wave is equal to or less than the time needed for one back-and-forth reverberation in the specimen. If the wave is longer, the build-up of stress during the second reverberation will cause plastic deformation. On the other hand, if the amplitude of the wave is higher, it will cause plastic deformation immediately when it reaches the specimen. There exists also a limiting amplitude below which the loading wave is unable to cause plastic deformation in the specimen regardless of the loading duration. In this case, even after complete build-up, the stress in the specimen is below the yield point.

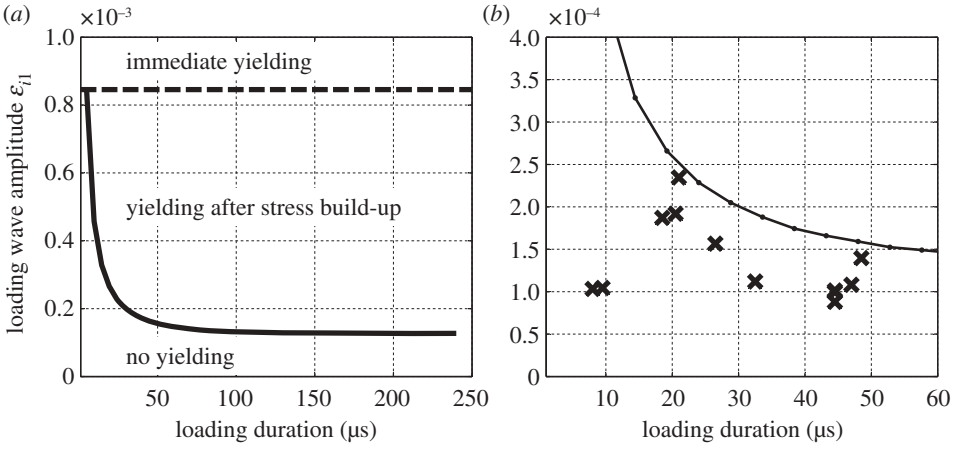


**Figure 7.** Incident bar residual wave amplitude–wave duration limit curves for a specimen similar to that used in the experimental tests: (*a*) full calculated region and (*b*) enlarged view of the most critical region; 'x' denotes incident bar residual wave peaks in the test shown in figure 6.

The experimental data shown in figure 6 were analysed using the method described above. The amplitudes and durations of the incident bar residual waves were determined using a rectangular search window. The lower detection threshold was set to $0.8 \times 10^{-4}$ bar strain, and the search window width was set so that peaks within 50 μs (corresponding to 10 wave reverberations in the specimen) from each other were counted as one wide peak. For a conservative approach, each detected peak was converted to a maximum amplitude–total duration pair in the subsequent analysis, i.e. the severity of the peak was overestimated. Figure 7*b* plots the results of the peak analysis in conjunction with the limit curve. As can be seen, all data points lie under the limit curve. The data points near the limit curve were individually checked by calculating the force in the specimen based on the actual record of the residual wave. It was found that these residual waves did not load the specimen above the yield strength. The analysis of the residual waves in conjunction with the post-test measurement of the specimen verifies that the recovery test was successful. Caution should, however, be exercised with the described calculation method, since it is based on *a priori* prediction of the effects of a given residual wave and the analysis may not correctly take into account other loading waves in the specimen during the actual arrival of the wave in question. This challenge can be approached by analysing a longer record of strain gauge data for signs of spurious high-amplitude waves and using additional means to measure the specimen deformation.

## 6. Conclusion

A new specimen recovery technique for a striker tube-based TSHB set-up is suggested. The technique is based on the use of two momentum trap bars in front of the incident bar. This eliminates the need for a precision-set gap between the incident bar and the traps, which is the most critical part of the existing techniques. Numerical simulations and experimental tests combined with residual wave analysis showed that the new technique improves the reliability of reflected wave trapping, which is the main contributor to the overall success of a recovery test. The most critical part of the new technique is ensuring good contact between the two momentum traps. This, however, is experimentally relatively simple to carry out, as demonstrated by the high success rate of the tests carried out with the new technique.

Acknowledgements. J. Kokkonen, T. Salomaa and K. Östman from Tampere University of Technology are acknowledged for their technical help with the experiments. S. Kilchert from the Fraunhofer Institute for High-Speed Dynamics is acknowledged for his help with the Abaqus simulations.

Funding statement. This work was supported by the FIMECC Ltd. (Finnish Metals and Engineering Competence Cluster) Demanding Applications Program and by Jenny and Antti Wihuri Foundation.

## Appendix A. Estimation of the length of the preset gap in the single trap method

According to the theory of uniaxial elastic stress waves, the particle speed $v$ and force $F$ within an elastic wave travelling in a slender bar are given by

$$v = -c_0\varepsilon \tag{A 1}$$

and

$$F = EA\varepsilon, \tag{A 2}$$

where $c_0$ is the travel speed of the wave, $\varepsilon$ is the strain caused by the wave (tensile strain is taken positive), while $E$ and $A$ are Young's modulus and cross-sectional area of the bar, respectively. Figure 8 shows a simplified description of the wave motion during the impact of the striker on the flange. The travel directions of the waves are indicated by the arrows in figure 8. It is assumed that, after several wave reflections within the flange, boundaries 'A' and 'B' are moving at the same velocity and that the force within the flange is zero. In this case, the amplitudes of the waves in the striker and the incident bar can be solved by assuming force balance and velocity continuity at the boundary 'A' in figure 8:

$$\sum F = EA_{\mathrm{str}}\varepsilon_{\mathrm{str}} + EA_{\mathrm{inci}}\varepsilon_{\mathrm{inci}} = 0 \tag{A 3}$$

and

$$v_{\mathrm{b}} = v_{\mathrm{a}} = -c_0\varepsilon_{\mathrm{inci}} = -c_0\varepsilon_{\mathrm{str}} - v_{0\mathrm{str}}. \tag{A 4}$$

It should be noted that, in this analysis, the material properties are assumed to be the same for all contacting parts. The distance $u_{\mathrm{b}}$ moved by the bar end is obtained by solving for $v_{\mathrm{b}}$ in equations (A 3) and (A 4) and integrating over impact time $\Delta t$, which is dependent on the striker length:

$$u_{\mathrm{b}} = \int_0^t v_{\mathrm{b}}\,\mathrm{d}t = -\frac{A_{\mathrm{str}}}{(A_{\mathrm{inci}} + A_{\mathrm{str}})}v_{0\mathrm{str}}\Delta t. \tag{A 5}$$

## Appendix B. Calculation method for the analysis of residual loading waves

Consider the case shown in figure 9. The specimen is in rigid contact with the incident and transmitted bars. All stress waves are assumed to be linear elastic. The basic equations and conventions are the same as in the analysis presented in appendix A. The calculation proceeds in steps $i$ that correspond to the time required for one back-and-forth reverberation within the specimen.

For time $t = i$, the force ($F$) balance and velocity ($v$) continuity equations for the boundaries 'A' and 'B' are given by

$$\sum F_{\mathrm{a}} = E_{\mathrm{inci}}A_{\mathrm{inci}}(\varepsilon_{i1}^{i} + \varepsilon_{i2}^{i}) - E_{\mathrm{spec}}A_{\mathrm{spec}}(\varepsilon_{s1}^{i} + \varepsilon_{s2}^{i-1}) = 0, \tag{B 1}$$

$$v_{\mathrm{a}} = -c_{\mathrm{inci}}(\varepsilon_{i1}^{i} - \varepsilon_{i2}^{i}) = -c_{\mathrm{spec}}(\varepsilon_{s1}^{i} - \varepsilon_{s2}^{i-1}), \tag{B 2}$$

$$\sum F_{\mathrm{b}} = E_{\mathrm{spec}}A_{\mathrm{spec}}(\varepsilon_{s1}^{i} + \varepsilon_{s2}^{i}) - E_{\mathrm{trans}}A_{\mathrm{trans}}\varepsilon_{t1}^{i} = 0 \tag{B 3}$$

and

$$v_{\mathrm{b}} = -c_{\mathrm{spec}}(\varepsilon_{s1}^{i} - \varepsilon_{s2}^{i}) = -c_{\mathrm{trans}}\varepsilon_{t1}^{i}, \tag{B 4}$$

where $E$, $A$ and $c$ denote Young's modulus, cross-sectional area and elastic wave speed of the components, respectively; and the subscripts inci, spec and trans denote incident bar, specimen and transmitted bar, respectively. Equations (B 1)–(B 4) form a set of four equations with four unknowns ($\varepsilon_{i1}$ is assumed prescribed) and thus an analytical solution can be found. It should be noted that at the boundary 'A' (equations (B 1) and (B 2)) the value obtained in the previous time

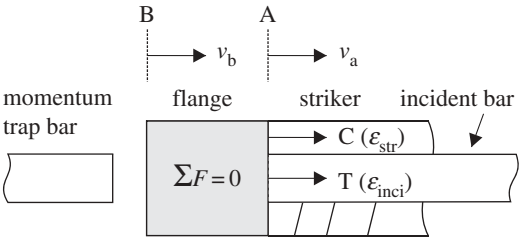


**Figure 8.** Schematic of the wave motion near the flange during striker impact in the single trap technique. 'C' and 'T' denote compression and tension stress waves, respectively.

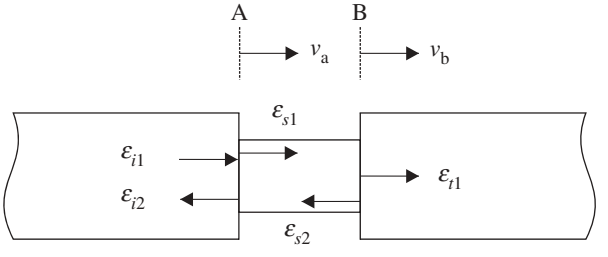


**Figure 9.** Linear elastic analysis of the waveform in an SHB specimen before yielding starts.

step $(i-1)$ for $\varepsilon_{s2}$ is used before it is updated at the boundary 'B'. This accounts for the physical back-and-forth motion of the stress wave within the specimen. From (B 1) and (B 2)

$$\varepsilon_{s1}^{i} = \left(c_{\text{spec}} + c_{\text{inci}}\frac{E_{\text{spec}}A_{\text{spec}}}{E_{\text{inci}}A_{\text{inci}}}\right)^{-1}\left(2c_{\text{inci}}\varepsilon_{i1}^{i} + \left(c_{\text{spec}} - c_{\text{inci}}\frac{E_{\text{spec}}A_{\text{spec}}}{E_{\text{inci}}A_{\text{inci}}}\right)\varepsilon_{s2}^{i-1}\right), \tag{B 5}$$

and from (B 3) and (B 4)

$$\varepsilon_{s2}^{i} = \left(E_{\text{spec}}A_{\text{spec}} + E_{\text{trans}}A_{\text{trans}}\frac{c_{\text{spec}}}{c_{\text{trans}}}\right)^{-1}\left(E_{\text{trans}}A_{\text{trans}}\frac{c_{\text{spec}}}{c_{\text{trans}}} - E_{\text{spec}}A_{\text{spec}}\right)\varepsilon_{s1}^{i}. \tag{B 6}$$

Based on the solutions (B 5) and (B 6), the axial force in the specimen during time step $t = i$ is given by

$$F_{\text{spec}}^{i} = E_{\text{spec}}A_{\text{spec}}(\varepsilon_{s1}^{i} + \varepsilon_{s2}^{i}). \tag{B 7}$$

Similar to the method presented by Parry *et al*. [8], equations (B 5)–(B 7) allow the evaluation of the force generated by an arbitrary-shaped incident pulse $\varepsilon_i(t)$. This feature can be used to evaluate the effects of individual residual stress waves, i.e. either to directly interpolate the strain gauge record between time steps $i$ in order to obtain $\varepsilon_{i1}$, or to use e.g. a trapezoidal pulse to mimic the shape of the actual wave. In addition, a limit curve can be calculated in order to analyse a larger set of residual waves. The limit curve describes those incident wave amplitude–duration pairs that are unable to cause plastic deformation in the specimen. For the calculation, it is assumed that the specimen is loaded by a rectangular incident wave with amplitude $\varepsilon_n$ and duration $t_n$ (in terms of the number of steps $i$). A series of pairs $(\varepsilon_n, t_n)$ is selected and for each pair equations (B 5)–(B 7) are iteratively calculated until $i = t_n$. Finally, the limit curve is obtained by finding those pairs $(\varepsilon_n, t_n)$ for which $F_{\text{spec}}$ remains below a level that causes plastic deformation in the specimen.

## References


1. Lezcano RG, Essa YE, Pérez-Castellanos JL. 2003 Numerical analysis of interruption process of dynamic tensile tests using a Hopkinson bar. *J. Phys. IV* **110**, 565–570. (doi:10.1051/jp4:20020753)
2. Essa YES, López-Puente J, Pérez-Castellanos JL. 2007 Numerical simulation and experimental study of a mechanism for Hopkinson bar test interruption. *J. Strain Anal. Eng.* **42**, 163–172. (doi:10.1243/03093247JSA206)
3. Ma D, Chen D, Wu S, Wang H, Hou Y, Cai C. 2010 An interrupted tensile testing at high strain rates for pure copper bars. *J. Appl. Phys.* **108**, 114902. (doi:10.1063/1.3516475)
4. Nemat-Nasser S, Isaacs JB, Starret JE. 1991 Hopkinson techniques for dynamic recovery experiments. *Proc. R. Soc. Lond. A* **435**, 371–391. (doi:10.1098/rspa.1991.0150)
5. Van Slycken J. 2008 Advanced use of a split Hopkinson bar setup application to TRIP steels. Doctoral thesis, Ghent University, Belgium.
6. Huang W, Huang Z, Zhou X. 2010 Loading and unloading split Hopkinson tension bar technique for studying dynamic microstructure evolution of materials. *Adv. Mater. Res.* **160–162**, 891–894. (doi:10.4028/www.scientific.net/AMR.160-162.891)
7. Prot M, Cloete TJ, Pattofatto S. 2012 Dynamic compression and recovery of cancellous bone for microstructural investigation. *EPJ Web Conf.* **26**, 03003. (doi:10.1051/epjconf/20122603003)
8. Parry DJ, Dixon PR, Hodson S, Al-Maliky N. 1994 Stress equilibrium effects within Hopkinson bar specimens. *J. Phys. IV* **4**, C8, 107–112. (doi:10.1051/jp4:1994816)
9. Frew DJ, Forrestal MJ, Chen W. 2001 A split Hopkinson pressure bar technique to determine compressive stress–strain data for rock materials. *Exp. Mech.* **41**, 40–46. (doi:10.1007/BF02323102)